Scientia Iranica C (2018) 25(3), 1323–1334

Sharif University of Technology
Scientia Iranica
Transactions C: Chemistry and Chemical Engineering
http://scientiairanica.sharif.edu

Ferric ion modified nano-MOF-5 synthesized by a direct mixing approach: A highly efficient adsorbent for methylene blue dye

A. Fallah Shojaei*, K. Tabatabaeian, and M. Zebardast

Department of Chemistry, Faculty of Sciences, University of Guilan, Rasht, P.O. Box 4193833697, Iran.

Received 21 December 2016; received in revised form 25 October 2017; accepted 23 April 2018

KEYWORDS
Adsorption kinetics;
Direct mixing approach;
Fe-MOF-5;
Isotherms;
Metal-organic framework;
Methylene blue.

Abstract. In this study, the adsorption of Methylene Blue (MB) dye was studied with modified Fe-MOF-5 and MOF-5 synthesized at room temperature by a direct mixing approach. The morphological and physicochemical properties of the prepared catalysts were characterized by Scanning Electron Microscopy (SEM), X-Ray Diffraction (XRD), and Fourier transform infrared spectroscopy (FT-IR). The removal rate of Fe-MOF-5 was considerably greater than that of MOF-5, showing that the adsorption performance of MOF-5 can improve through necessary modifications. The influence of various parameters on the adsorption interaction of the prepared compounds was considered in pH value, contact time, temperature, adsorbent dosage, and concentration of MB. Consequently, the adsorption kinetics, thermodynamics, and isotherms were explored consistently. To predict the adsorption isotherms and specify the characteristic parameters for the process design, four isotherm models, such as Langmuir, Freundlich, Temkin, and Dubinin-Radushkevich (D-R), were applied. The experimental isotherm data were found to fit the Langmuir model properly. Additionally, adsorption kinetic data were tested using pseudo-first-order, pseudo-second-order, and Elovich models and were found to fit pseudo-second-order model. The thermodynamic parameters illustrated that the adsorption was a spontaneous and endothermic process.

1. Introduction

Metal-Organic Frameworks (MOFs) represent an appealing class of highly porous hybrid materials constructed by metal-containing nodes connected by various organic bridges which bear multiple complex functions [1]. In comparison with conventional adsorbents, strong points of MOFs include diverse compositions and structure types, tunable pore size, large surface area, and coordinatively unsaturated/saturated metal sites to regulate the adsorption ability [2]. MOFs have presented a great potential in sorption-related fields, too [3]. Therefore, MOFs have been widely explored for gas storage, capture of green-house gases [4], as well as adsorption of volatile organic compounds up to now [5]. Moreover, the adsorption and removal of pharmaceuticals (naproxen and clofibric acid) [6], dyes [7], alkyl aromatics and phenols [8], pesticides [9], nitrogen and sulfur compounds [10] from the liquid phase have been also reported. Although the research on aqueous adsorption of contaminants on MOFs is limited, the recent studies have paved the way for wide applications of MOFs in removal and adsorption of contaminants from polluted aqueous environment [11].

MB, as a cationic azo dye, exists extensively in

*. *Corresponding author.*
E-mail address: a-fallah@guilan.ac.ir (A. Fallah Shojaei)

doi: 10.24200/sci.2018.20336

wastewater produced by textile, leather tanning, and paper industries [7]. MB deteriorates water quality and makes a significant impact on human health due to poisonous, carcinogenic, mutagenic or teratogenic effects. Therefore, the removal of MB from contaminated water is a very attractive subject [12].

Nowadays, various methods are being developed to remove MB from aqueous solutions, including photodegradation, biodegradation, and adsorption [13]. The adsorption method is appealing for the removal of dyes, because dye is quite stable against light and heat as well as is resistant to oxidation and biodegradation [8]. Besides, the sorption technique works effectively without any additional pre-treatment before utilization [14]. Activated Carbons (AC) and zeolites are well-studied classes of materials for the adsorption of MB from water [15]. Though AC and zeolites have been used extensively in the removal of MB, the adsorption capacity is quite limited [13].

Among the numerous MOFs reported so far, MOF-5's potential applications have been largely studied [16]. MOF-5, for which the chemical formula is $Zn_4O[C_6H_4(CO_2)_2]$, has a cubic structure, average pore diameter of 18.6 Å, and huge pore size ($<$ 20 Å diameter pore size) coming up with fairly good sorption for gaseous hydrogen [17]. However, up to now, there has not been any report about the application of MOFs, including Fe-BDC (Fe-MOF-5), in the adsorption of dyes nor any kinetic and thermodynamic studies in this context as well as any related kinetic and thermodynamic studies. This study, for the first time, exposes the efficient adsorption and removal of MB from aqueous solution by Fe-MOF-5 synthesized at room temperature and just in a few hours. The adsorption behavior of MB on Fe-MOF-5 was studied in respect of factors potentially affecting the adsorption, adsorption isotherms, kinetics, thermodynamics, and mechanism.

2. Experimental

2.1. Materials

All reagents and starting materials were procured commercially from Merck and used as received without further purification unless otherwise noted.

2.2. Preparation of the adsorbents

Modified Fe-MOF-5 nanocrystals were synthesized according to the associated literature with slight modifications [18]. Briefly, a solid mixture of iron (III) nitrate hexahydrate $[Fe(NO_3)_3.6H_2O]$ (1.2 g) and 1,4-benzene dicarboxylic acid (0.334 g) (H_2BDC) was dissolved in N,N-dimethylformamide (DMF, 40 mL)) under vigorous stirring followed by the addition of 2.2 mL triethylamine (TEA) dropwise. The mixture was stirred for an hour until a brownish precipitate was formed. The precipitate was filtered and washed with DMF as well as chloroform (3×10 mL). The solid was finally dried in a vacuum condition at 80°C for 6 h.

Nano-sized MOF-5 was achieved by modified procedures reported by Li [19]. About 1.2 g of zinc nitrate hexahydrate $[Zn(NO_3)_2.6H_2O]$ and 0.334 g of H_2BDC were dissolved in 40 mL of DMF under constant agitation in atmospheric conditions. 2.2 mL of TEA was added drop by drop when a colorless solution was being formed. After stirring for one hour, a white product was filtered and washed several times with DMF and chloroform (3×10 mL). The solid product was finally dried in a vacuum condition at 80°C for 6 h.

2.3. Characterization

SEM images were obtained on a Philips, XL30 instrument operating at 26 kV. The XRD data were collected using a D8 Bruker advanced diffractometer with Cu-K_α radiation, scan rate of 0.1 2θ/s, and within the range of 2-50°. FT-IR spectra were recorded in the range of 400-4000 cm^{-1} on a Bruker Vector 22 FT-IR spectrophotometer utilizing KBr plates.

2.4. Adsorption studies

The adsorption was performed by batch experiments. An aqueous stock solution of MB (1000 ppm) was prepared by dissolving MB ($C_{16}H_{18}ClN_3S$, MW: 373.9) in deionized water. MB calibration curve was prepared by determining the absorbance at 664 nm (λ_{max}) with a series of standard MB solutions (2-14 ppm) at neutral pH, and the initial or equilibrium concentrations of MB were calculated with the calibration curve. Prior to adsorption, the adsorbents were dried overnight at 100°C in a vacuum condition. For each test, approximately 25 mg of the sample was added to the MB solution (25 mL, fixed concentration, pH: 7) and stirred for 10 min to 160 min at 298 K. Then, the adsorbents were filtered by centrifugation, and the MB concentration was determined from the absorbance of the UV spectra of the solutions with a spectrophotometer (UV-1800 RAILEGH). Adsorption isotherm tests were carried out by a series of initial concentrations (100-500 mg/L). To calculate the thermodynamic properties, adsorption isotherms were recorded in 25 mL of MB solution at 298, 303, and 313 K. The adsorption kinetic experiment was carried out by the adsorption procedure, which was mentioned before, at certain intervals of time with 25 mL solutions (100-500 mg/L).

The MB removal percentage over the adsorbents was calculated by Eq. (1) [20]:

$$\text{Removal } (\%) = \frac{C_0 - C_e}{C_0} \times 100, \tag{1}$$

where C_0 (mg/L) and C_e are the initial and equilibrium solution concentrations, respectively.

The equilibrium uptake was calculated by Eq. (2)

[20]:

$$q_e = \frac{V}{m}(C_0 - C_e), \tag{2}$$

where q_e (mg/g) is the equilibrium adsorption capacity of the adsorbent, and V (L) and m (g) are the volume of the solution and the weight of the adsorbents, respectively.

To determine the adsorption capacity at various pHs, the pH of the MB solutions was adjusted to 0.1 M HCl or 0.1 M NaOH aqueous solution. The adsorption rate constant was calculated using pseudo-second or pseudo-first-order reaction kinetics [21]. The maximum adsorption capacity was accounted using the Langmuir adsorption isotherm [13].

3. Results and discussion

3.1. Synthesis and characterization of the adsorbents

Modified nano Fe-MOF-5 was characterized and prepared by the direct mixing approach in an atmospheric condition. The morphology and particle size of the samples were considered by SEM, as shown in Figure 1. The MOF-5 morphology is characterized by nanospheres crystals of 40-70 nm in diameter (Figure 1(a)). As shown in Figure 1(b), Fe-MOF-5 nanocrystals display irregular nanospheres' morphology with the average particle size of 30-50 nm. Furthermore, adding TEA to the liquid phase results in spherical nanocrystals, consistent with the reported data in literature [3].

The XRD pattern in Figure 2(a) shows that the overall patterns seem to be similar to the results shown by Li [22], Huang [23], and Hafizovic [24]. However, a key peak (2θ of 6.8°) is missing in the present study, probably, due to some alterations of atomic orientation in crystal surface by a solvent and other adsorbate molecules that fill the pores of MOF-5s [23]. The diffraction peaks of Fe-MOF-5 are almost the same as those of MOF-5, suggesting that crystal structure remains intact [22].

FT-IR spectra of the prepared samples are shown in Figure 2(b) while confirming the presence of the required functional groups. The bands at around 1381 and 1578 cm^{-1} are the symmetric and asymmetric characteristic stretching vibrations of the carboxylate in BDC^{2-} [25]. Several weak absorptions seen in the region of 600-800 cm^{-1} are the result of the out-of-plane bending vibrations of the aromatic C-H groups of the benzene ring present in H_2BDC [25]. The broad band around 3200-3500 cm^{-1} is due to the adsorbed moisture content [26]. Both MOF-5 and Fe-MOF-5, synthesized by the direct mixing approach, do not show the absorption of protonated BDC around 1715-1680 cm^{-1}, confirming the complete deprotonation of H_2BDC by TEA in MOF-5 and coordination between the linker and ferric ion in Fe-MOF-5 [27].

3.2. MB adsorption

3.2.1. Comparison of removal rate for different initial concentration of MB in Fe-MOF-5 and MOF-5

The initial concentration is an important factor which provides an essential driving force to avoid mass transmission resistance of the molecules between the adsorbent and the aqueous [28]. The adsorption behaviors of MOF-5 and Fe-MOF-5 towards MB with different initial concentrations are compared, as shown in Figure 3. Apparently, the removal rate of Fe-MOF-5 toward MB is high, even in the first 40 min at a lower initial concentration (4 mg/L, 10 mg/L and 12 mg/L). However, by the initial concentration increase of MB up to 16 mg/L, the removal rate of Fe-MOF-5 decreases more than lower concentrations.

3.2.2. Contact time effect

To explore the adsorption process, effect of the contact time increase on the adsorption capacity is calculated and shown in Figure 4(a). It is observed that the uptake is done rapidly in the first stage through 0 to 80 min. The second stage can be described at the

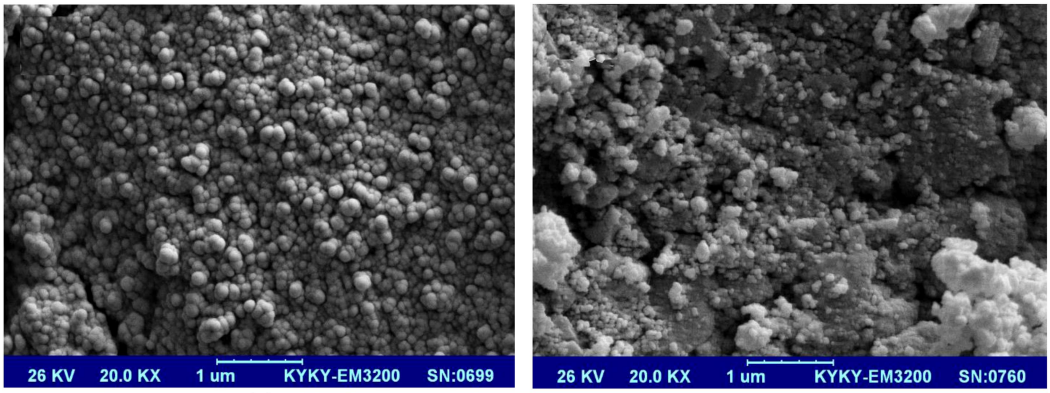

(a) (b)

Figure 1. SEM images of (a) MOF-5 and (b) Fe-MOF-5.

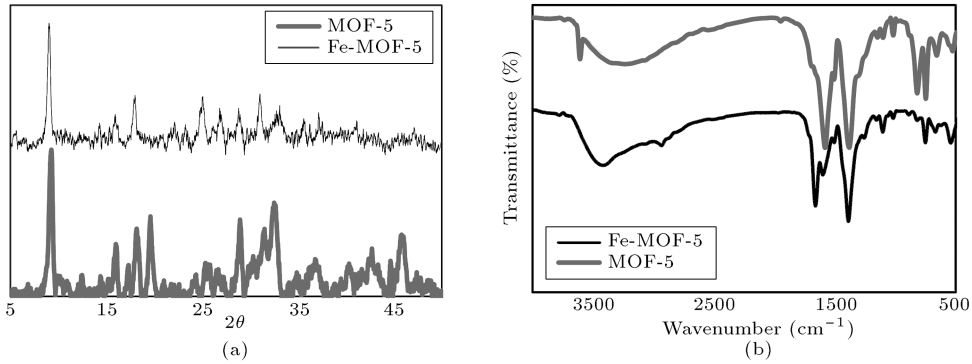

Figure 2. XRD patterns (a) and FT-IR spectra (b) of MOF-5 and Fe-MOF-5.

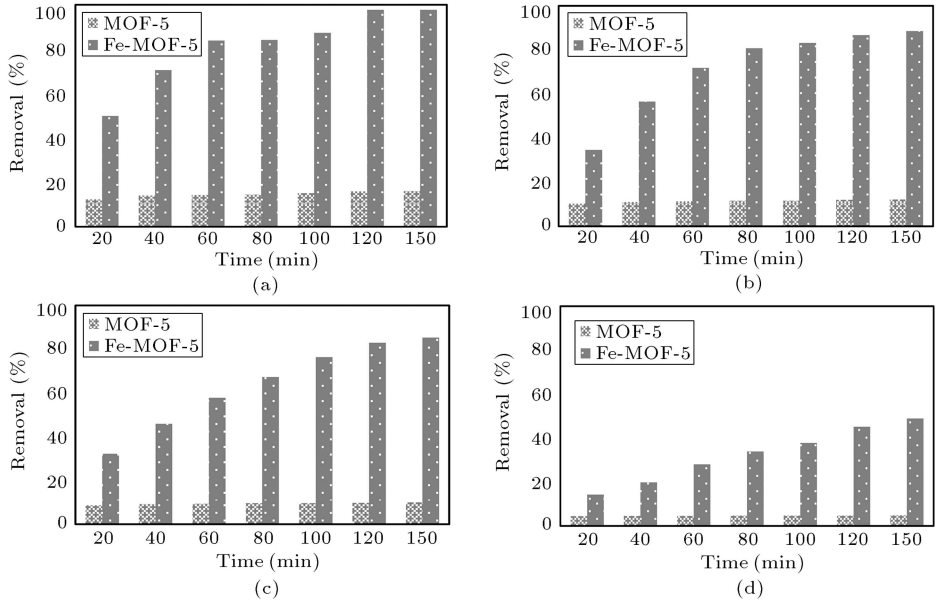

Figure 3. Comparison of removal rates for MB in $C_0 = 4$ mg/L (a), 10 mg/L (b), 12 mg/L (c) and 16 mg/L (d); $m = 25$ mg; $V = 25$ mL.

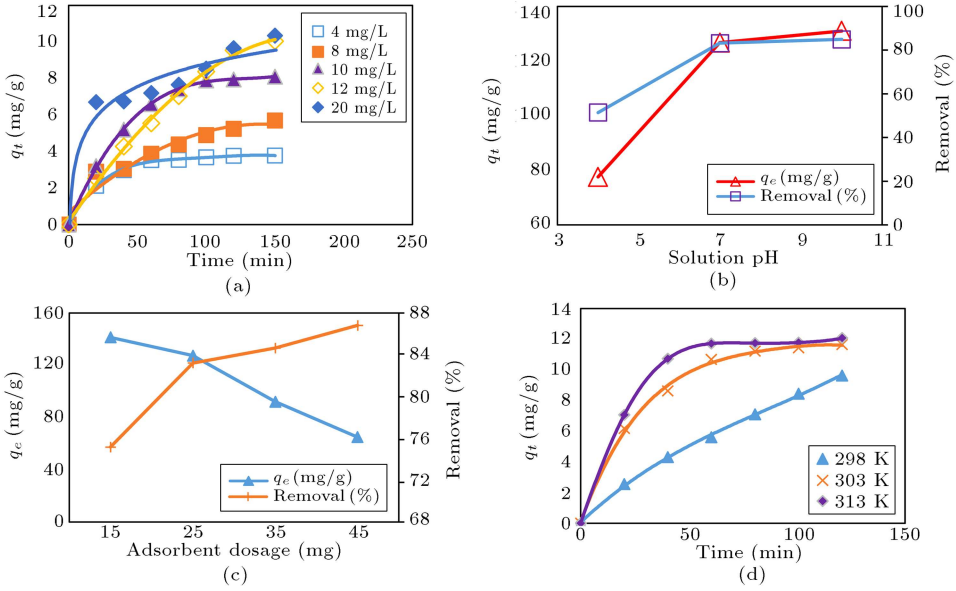

Figure 4. Effect of (a) contact time, (b) solution pH, (c) adsorbent dosage, and (d) temperature on uptake of MB to Fe-MOF-5.

lower rate of 80 to 120; then, the process reaches the saturated state. To justify this phenomenon, probably, there are more attainable vacant surface sites in Fe-MOF-5 throughout the initial stage, leading to MB molecules that are adsorbed rapidly on the outer surface [29]. Furthermore, the MB uptake increases with increasing initial concentration of MB, demonstrating the favorable adsorption of MB due to the increase of the number of collisions among the adsorbents and the dye ions at a high concentration [29].

3.2.3. Effect of the solution pH

The pH impresses dye adsorption by changing the surface charge of the adsorbent as well as the specific distribution of dye in the solution phase [30]. As shown in Figure 4(b), the MB adsorption onto Fe-MOF-5 is sensitive to the pH of the solution. The amount of MB adsorbed onto Fe-MOF-5 increases from 77.53 to 131 mg/g with the pH increasing from 4 to 10. This phenomenon could be explained by the dissociation of carboxylate groups (-COOH) on Fe-MOF-5 surface [30]. Electrostatic attraction between the MB cations and the negatively charged sites on the surface of Fe-MOF-5 is considered a major driving force for the adsorption. Therefore, increasing pH of the solution enhances the adsorption.

3.2.4. Effect of adsorbent dosage

Figure 4(c) shows the effects of Fe-MOF-5 dosage on the adsorption of MB. The removal percentage of MB increases as Fe-MOF-5 dosage increases. However, when the adsorbent dose increases more than before, the removal percentage increases slightly. Furthermore, it can be seen that, by increasing the adsorbent dose, the adsorption capacity of MB decreases. It is mainly due to a higher adsorbent dosage which provides a large excess of the active sites leading to the lower utility of the sites at a certain concentration of MB [30].

3.2.5. Effect of temperature

Figure 4(d) shows the relationship between the adsorption capacity (q_t) and MB concentration in solution at different temperatures (298, 308, and 318 K). Obviously, the temperature remarkably influences the adsorption of MB. By increasing temperature, the adsorption capacity increases, indicating that the adsorption is an endothermic process and high temperature assists the adsorption. Increasing temperature may cause a swelling effect on the porosity and the pore volume of the adsorbent which enables MB molecules to permeate rapidly across the surface and within the internal pores of the adsorbent [30].

3.3. Adsorption isotherm

Adsorption isotherm models are widely utilized to describe the adsorption progress and investigate adsorption mechanisms. Thus, the equilibrium data of Fe-MOF-5 fit the Langmiur, Freundlich, Temkin, and D-R isotherm models. The application of isotherm models to the adsorption treatment was studied by judging the correlation coefficient (R^2). Langmuir isotherm is based on the theory that the adsorption process occurs at specific homogeneous sites onto the adsorbent surface. Moreover, when a dye molecule occupies a site, there is no possibility for further adsorption to at that site. In other words, it is deduced that the adsorption process is of the monolayer naturally. The linear form of the Langmuir isotherm model is expressed by Eq. (3) [12]:

$$\frac{C_e}{q_e} = \frac{1}{q_m K_L} + \frac{C_e}{q_m}, \tag{3}$$

where C_e is the equilibrium concentration of adsorbate (mg/L), q_e is the equilibrium adsorption capacity (mg/g), q_m is the maximum adsorption capacity of the adsorbate (mg/g), and K_L (L/mg) is a Langmuir constant related to the affinity of the binding sites and energy of adsorption. The high value of R^2 indicates that the adsorption of MB onto Fe-MOF-5 follows the Langmuir isotherm model. A linear relation is obtained between C_e/q_e and C_e (Figure 5); the Langmuir isotherm constants (K_L and q_m) are shown in Table 1.

For predicting the favorability of an adsorption system, the Langmuir equation can also be remarked in terms of a dimensionless separation factor, R_L, defined in Eq. (4) [12]:

$$R_L = \frac{1}{1 + K_L C_m}, \tag{4}$$

where C_m is the maximum initial concentration of adsorbate. R_L indicates the favorability and capacity of adsorption system. When $0 < R_L < 1.0$, it represents favor adsorption [31]. R_L values are in the

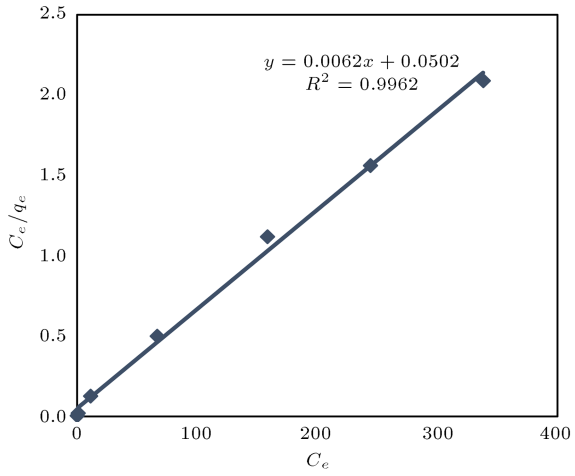

Figure 5. Linear plot of Langmuir isotherm of MB adsorption onto Fe-MOF-5.

Table 1. Langmuir, Freundlich, Temkin and *D-R* constants for the adsorption of MB onto Fe-MOF-5 ($m = 25$ mg; $V = 25$ mL; pH = 7.0, $T = 298$ K; contact time = 7h).

Isotherm model	Parameter	Value	R^2
Langmuir	K_L (L/mg)	0.123	0.9962
	$Q_{\max}$ (mg/g)	161.29	
Freundlich	K_F (mg/g)	59.829	0.972
	n	5.8	
	$1/n$	0.1724	
Temkin	B_T	117.811	0.984
	b_T	21.03	
	K_t	6.404	
D-R	β	0.0027	0.956
	q_m	154.578	
	E_a	13.608	

range of 0.016-0.168 which proves that the adsorption is a favorable process. Moreover, R_L value is approximately zero when C_0 increases, which means that the sorption of MB onto Fe-MOF-5 is less favorable at a high initial MB concentration [13].

The corresponding Freundlich, Temkin, and *D-R* parameters are shown in Appendix A, and the values of their parameters are calculated and listed in Table 1.

To calculate the sorption energy, *D-R* isotherm model was used. The amount of mean adsorption energy gives information about chemical and physical adsorptions. The numerical value of E_a (Table 2) was calculated as 13.6 KJ/mol. According to the literature [30], the value of E_a is in the range of 8 to 16 kJ/mol which indicates the chemical adsorption process.

As shown in Table 2, Langmuir isotherm fits appropriately the experimental data (correlation coefficient $R^2 > 0.99$). This indicates that the Langmuir model is very suitable for describing the adsorption equilibrium of MB onto Fe-MOF-5. The maximum adsorption capacity of MB onto Fe-MOF-5 (q_0) is 161.29 mg/g at 298 K. The fact that the Langmuir isotherm fits the experimental data very well may be due to the homogeneous distribution of active sites on the Fe-MOF-5 surface, since the surface is homogeneous as considered by the Langmuir equation [13]. The utilization of the isotherm equation to describe the adsorption process was judged by R^2. The adsorption isotherm models fitted the data, based on R^2 values, in the order of Langmuir > Temkin > Freundlich > *D-R* isotherm. The value of Freundlich constant n larger than 1 points to the favorable sorption candidates.

3.4. Adsorption kinetics

To analyze the kinetics of MB adsorption onto Fe-MOF-5, the pseudo-first-order, pseudo-second-order, Elovich and intraparticle diffusion models were examined at three different initial MB concentrations in this study. The pseudo-first-order model was applied to the adsorption process, described in Appendix B. The related parameters are presented in Table 2. There is a significant difference between calculated q_e and experimental q_e.

The pseudo-second-order equation can be expressed by Eq. (5) [27]:

$$\frac{t}{q_t} = \frac{1}{k_2 q_e^2} + \frac{t}{q_e}, \tag{5}$$

where k_2 (g/mg.min) is the rate constant of pseudo-second-order adsorption determined by plotting t/q_t versus t at different initial MB concentrations, as shown in Figure 6(a), and the values of parameters are summarized in Table 2. The data display excellent agreement of the pseudo-second-order model with high R^2 ($R^2 > 0.99$). Moreover, because the calculated q_e values are very close to the measured one [27], the good agreement mentioned above can be confirmed.

The Elovich equation was first developed to describe the kinetics of chemisorption of gas onto solids [27] (Appendix B). It is possible that the kinetic data are analyzed by the intraparticle diffusion kinetic model, written as in Eq. (6) [28]:

$$q_t = k_d t^{\frac{1}{2}} + C, \tag{6}$$

Table 2. A comparison of pseudo-first-order (a), pseudo-second-order (b), Elovich (c), and intraparticle diffusion (d) kinetic models' rate constants calculated from experimental data.

C_0	$Q_{e,exp}$	Pseudo-first-order kinetic model			Pseudo-second-order kinetic model			Elovich kinetic model			Intraparticle diffusion model		
(mg/L)	(mg/g)	K_1 (min^{-1})	$Q_{e,cal}$ (mg/g)	R^2	K_2 (g/mg.min)	$Q_{e,cal}$ (mg/g)	R^2	α	β	R^2	k_d (mg/g $min^{1/2}$)	C	R^2
100	85.94	0.015	161.47	0.731	1.15	104.16	0.974	2.97	0.043	0.957	3.5 89	20.11	0.943
200	104.64	0.013	84.85	0.9569	1.87	119.04	0.994	13.45	0.048	0.92	3.222	47.974	0.886
300	98.904	0.0007	27.82	0.9929	4.64	104.66	0.998	340.69	0.093	0.986	3.589	20.119	0.943
400	107.64	0.008	49.96	0.7535	2.87	114.94	0.993	101.06	0.074	0.91	2.133	66.886	0.917

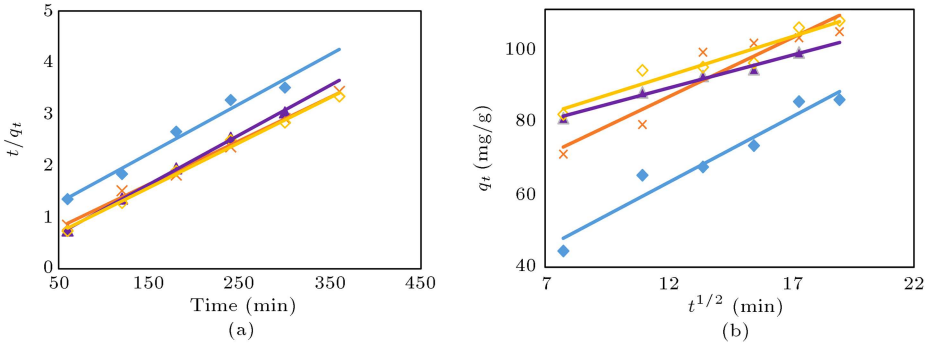

Figure 6. Linear plots of (a) pseudo-second-order and (b) intraparticle diffusion kinetic models of MB adsorption onto Fe-MOF-5 (C_0 = ♦100 mg/L, ■ 200 mg/L, ▲ 300 mg/L, ◊ 400 mg/L).

where k_d is the intraparticle diffusion rate constant (mg/g $\text{min}^{1/2}$), and C is a constant. The values k_d, C and correlation coefficient calculated from the slope of the plots of q_t versus $t^{1/2}$ are shown in Table 2 and Figure 6(b). It is discovered that the correlation coefficients for the intraparticle diffusion model are above 0.88, indicating a rich description for MB adsorption by this kinetic model. The value of intercept exposes an idea about the boundary layer thickness, i.e. the greater the intercept, the larger the boundary layer effect [13]. It is clearly observed from Table 2 that the intercepts are not zero but large values which increase with increasing initial MB concentrations for MB adsorption onto Fe-MOF-5. This result implies that boundary layer diffusion may be the rate-limiting step in the adsorption process for Fe-MOF-5 and is more dominant when the initial MB concentration is higher.

3.5. Adsorption thermodynamics

Thermodynamic parameters, containing changes in the Gibbs free energy (ΔG°), enthalpy (ΔH°), and entropy (ΔS°) for the adsorption of MB onto Fe-MOF-5, are determined based on the distribution coefficient (k_d) of solute between the solid and liquid phases [32]. The values of ΔG°, ΔH°, and ΔS° are calculated using the following equations [32]:

$$K_d = \frac{q_e}{C_e}, \tag{7}$$

$$\Delta G^\circ = -RT \ln K_d, \tag{8}$$

$$\ln K_d = -\frac{\Delta G^\circ}{RT} = -\frac{\Delta H^\circ}{RT} + \frac{\Delta S^\circ}{R}, \tag{9}$$

where K_d is the distribution coefficient of the adsorbent equal to q_e/C_e. The values of ΔS° and ΔH° were calculated aboard the intercept and slope of the Van't Hoff plot of $\ln K_d$ versus $1/T$, respectively.

The values of the thermodynamic parameters for MB adsorption onto Fe-MOF-5 are listed in Table 3. The negative values of ΔG° at various temperatures demonstrated the feasibility of the process and spontaneous nature of the adsorption. In addition, the negative amount of ΔG° decreased with increasing temperature, representing that the spontaneous nature of adsorption of MB is commensurate to the temperature. The value of ΔH° is positive, suggesting that the reaction is endothermic which is in agreement with the consequence of temperature-based MB uptake increases. The positive value of ΔS° indicates that the adsorption is irreversible [32].

3.6. Adsorption mechanism

Even though a more detailed study is necessary to clarify the mechanism of MB adsorption on modified Fe-MOF-5, the adsorption may be explained by an electrostatic interaction between the dye and adsorbent [33]. MB exists in the positive form; therefore, there will be an electrostatic interaction between the dye and adsorbent having a negative charge. As explained above, when the pH increases from 4 to 10, the amount of MB adsorbed onto Fe-MOF-5 increases from 77.53 to 131 mg/g, which displays the role of electrostatic interaction in the adsorption process.

Possibly, Fe^{3+} is more effective than Zn^{2+} because of its higher electronegative attribute. In other words, its ionized connection aspect with O^{2-} of carboxylate is higher. Thus, it rises anionic aspect of carboxylate and facilitates cationic dye adsorption since Fe is more electronegative and effective than Zn.

However, the possibility of another mechanism, such as π-π interaction [34], between benzene rings of

Table 3. Thermodynamic parameters for the adsorption of MB on Fe-MOF-5.

ΔH° (KJ/mol)	ΔS° (J/mol.K)	ΔG° (KJ/mol)		
		298 K	308 K	318 K
83.164	292.262	-3.956	-7.275	-9.761

Table 4. Previous studies on MB adsorption and the maximum amounts adsorbed.

Adsorbent	pH	Temp. (K)	q_m (mg/g)	Ref.
Clay	7.0	298	60	[35]
Natural zeolite	5.0	298	23.6	[36]
Modified zeolite	7.0	298	42.7	[37]
Hazelnut shell	4.1-4.5	298	96	[38]
Activated carbon	7.0	298	46.3	[39]
Graphene	3.0	293	153.85	[40]
Graphene oxide/calcium alginate	5.4	298	181.81	[40]
MOF-199	7.0	298	15.28	[41]
Fe_3O_4@MIL-100(Fe)	7.0	298	49.41	[42]
Fe_3O_4@MIL-100(Fe)	7.0	318	73.80	[42]
Fe-MOF-5	**7.0**	**298**	**161.29**	**This work**

Fe-MOF-5 and MB cannot be ruled out. Preliminary experiments indicate that Fe-MOF-5 may have potential applications in adsorption of MB.

3.7. Comparison of other adsorbents

Apparently, a direct comparison of Fe-MOF-5 with those obtained in literature is not feasible because of different experimental conditions utilized in those studies. The data in Table 4 show that synthesized Fe-MOF-5 in this study has comparable adsorption capacity compared to many adsorbents.

4. Conclusion

Modified nano-sized Fe-MOF-5 and MOF-5 nanocrystals were synthesized by the direct mixing approach at room temperature and characterized by SEM, XRD, and FT-IR techniques and used in the removal of MB from aqueous solutions. Furthermore, kinetics, isotherm, and thermodynamics of adsorption were explored fully. The adsorption process of MB fitted the pseudo-second-order kinetic model completely. The Langmuir isotherm model yielded much better agreement with it than Temkin, Freundlich, and *D-R* did. The MB maximum adsorption capacity of Fe-MOF-5 calculated from the Langmuir model is 161.29 mg/g at 298 K and is strongly dependent on the adsorbent dosage, pH, temperature, contact time, and initial concentration. The thermodynamic parameters demonstrated that the adsorption was a spontaneous and endothermic process. Despite the mediocre adsorption capacity of the Fe-MOF-5 compared with some adsorbents, it is acceptable to use it as an adsorbent regarding the mentioned characteristics. Additionally, Fe-MOF-5 utilization as an adsorbent has several advantages making it worthy: low cost and easy production, synthesis in room temperature conditions, and time saving.

Acknowledgement

The financial support of this work by University of Guilan research council is gratefully acknowledged.

References

1. Yaghi, O.M., O'Keeffe, M., Ockwig, N.W., Chae, H.K., Eddaoudi, M., and Kim, J. "Reticular synthesis and the design of new materials", *Nature*, **423**(6941), pp. 705-714 (2003).
2. Liu, J., Chen, L., Cui, H., Zhang, J., Zhang, L., and Su, C.-Y. "Applications of metal-organic frameworks in heterogeneous supramolecular catalysis", *Chem. Soc. Rev.*, **43**(16), pp. 6011-6061 (2014).
3. Li, J.R., Sculley, J., and Zhou, H.C. "Metal-organic frameworks for separations", *Chem. Rev.*, **112**(2), pp. 869-932 (2012).
4. Sumida, K., Rogow, D.L., Mason, J.A., McDonald, T.M., Bloch, E.D., Herm, Z.R., Bae, T.H., and Long, J.R. "Carbon dioxide capture in metal-organic frameworks", *Chem. Rev.*, **112**(2), pp. 724-781 (2012).
5. Huang, C., Song, M., Gu, Z., Wang, H., and Yan, X. "Probing the adsorption characteristic of metal-organic framework MIL-101 for volatile organic compounds by quartz crystal", *Envir. Sci. Tech.*, **45**, pp. 4490-4496 (2011).
6. Seo, P.W., Bhadra, B.N., Ahmed, I., Khan, N.A., and Jhung, S.H. "Adsorptive removal of pharmaceuticals and personal care products from water with functionalized metal-organic frameworks: remarkable adsorbents with hydrogen-bonding abilities", *Sci. Rep.*, **6**, pp. 2044-2051 (2016).
7. Lin, S., Song, Z., Che, G., Ren, A., Li, P., Liu, C., and Zhang, J. "Adsorption behavior of metal-organic

frameworks for methylene blue from aqueous solution", *Micropor. Mesopor. Mat.*, **193**, pp. 27-34 (2014).

8. Xie, L., Liu, D., Huang, H., Yang, Q., and Zhong, C. "Efficient capture of nitrobenzene from waste water using metal-organic frameworks", *Chem. Eng. J.*, **246**, pp. 142-149 (2014).
9. Kumar, P., Paul, A.K., and Deep, A. "Sensitive chemosensing of nitro group containing organophosphate pesticides with MOF-5", *Micropor. Mesopor. Mat.*, **195**, pp. 60-66 (2014).
10. Wang, X.L., Fan, H.L., Tian, Z., He, E.Y., Li, Y., and Shangguan, J. "Adsorptive removal of sulfur compounds using IRMOF-3 at ambient temperature", *Appl. Surf. Sci.*, **289**, pp. 107-113 (2014).
11. Huo, S.-H. and Yan, X.-P. "Metal-organic framework MIL-100(Fe) for the adsorption of malachite green from aqueous solution", *J. Mater. Chem.*, **22**, pp. 7449-7455 (2012).
12. Culp, S.J. and Beland, F.A. "Malachite green: A toxicological review", *Int. J. Toxicol.*, **15**(3), pp. 219-238 (1996).
13. Rafatullah, M., Sulaiman, O., Hashim, R., and Ahmad, A. "Adsorption of methylene blue on low-cost adsorbents: A review", *J. Hazard. Mater.*, **177**(1), pp. 70-80 (2010).
14. Wang, B., Lv, X.L., Feng, D., Xie, L.H., Zhang, J., Li, M., Xie, Y., Li, J.R., and Zhou, H.C. "Highly stable Zr(IV)-based metal-organic frameworks for the detection and removal of antibiotics and organic explosives in water", *J. Am. Chem. Soc.*, **138**(19), pp. 6204-6216 (2016).
15. MiarAlipour, S., Friedmann, D., Scott, J., and Amal, R. "TiO_2/porous adsorbents: Recent advances and novel applications", *J. Hazard. Mater.*, **341**, pp. 404-423 (2018).
16. Opelt, S., Türk, S., Dietzsch, E., Henschel, A., Kaskel, S., and Klemm, E. "Preparation of palladium supported on MOF-5 and its use as hydrogenation catalyst", *Catal. Commun.*, **9**(6), pp. 1286-1290 (2008).
17. McGaughey, A.J.H. and Kaviany, M. "Thermal conductivity decomposition and analysis using molecular dynamics simulations. Part II. Complex silica structures", *International J. Heat Mass Transf.*, **47**(8), pp. 1799-1816 (2004).
18. Cele, M.N., Friedrich, H.B., and Bala, M.D. "Liquid phase oxidation of n-octane to C8 oxygenates over modified Fe-MOF-5 catalysts", *Catal. Commun.*, **57**, pp. 99-102 (2014).
19. Li, J., Cheng, S., Zhao, Q., Long, P., and Dong, J. "Synthesis and hydrogen-storage behavior of metal-organic framework MOF-5", *Int. J. Hydrogen Energ.*, **34**(3), pp. 1377-1382 (2009).
20. Li, Y., Zhang, S., and Song, D. "A luminescent metal-organic framework as a turn-on sensor for DMF vapor", *Angew. Chemie. - Int. Ed.*, **52**, pp. 710-713 (2013).
21. Ho, Y.S. and McKay, G. "Pseudo-second order model for sorption processes", *Process Biochem.*, **34**(5), pp. 451-465 (1999).
22. Li, H., Eddaoudi, M., O'Keeffe, M., and Yaghi, O.M. "Design and synthesis of an exceptionally stable and highly porous metal-organic framework", *Nature*, **402**(6759), pp. 276-279 (1999).
23. Huang, L. "Synthesis, morphology control, and properties of porous metal-organic coordination polymers", *Micropor. Mesopor. Mat.*, **58**(2), pp. 105-114 (2003).
24. Hafizovic, J., Bjørgen, M., Olsbye, U., Dietzel, P.D.C., Bordiga, S., Prestipino, C., Lamberti, C., and Lillerud, K.P. "The inconsistency in adsorption properties and powder XRD data of MOF-5 is rationalized by framework interpenetration and the presence of organic and inorganic species in the nanocavities", *J. Am. Chem. Soc.*, **129**(12), pp. 3612-3620 (2007).
25. Sabouni, R., Kazemian, H., and Rohani, S. "A novel combined manufacturing technique for rapid production of IRMOF-1 using ultrasound and microwave energies", *Chem. Eng. J.*, **165**(3), pp. 966-973 (2010).
26. Khan, J., Rades, T., and Boyd, B.J. "Lipid-based formulations can enable the model poorly water-soluble weakly basic drug cinnarizine to precipitate in an amorphous-salt form during in vitro digestion", *Mol. Pharm.*, **13**, pp. 3783-3793 (2016).
27. Reineke, T.M., Eddaoudi, M., Fehr, M., Kelley, D., and Yaghi, O.M. "From condensed lanthanide coordination solids to microporous frameworks having accessible metal sites", *J. Am. Chem. Soc.*, **121**(8), pp. 1651-1657 (1999).
28. Liu, X., Luo, J., Zhu, Y., Yang, Y., and Yang, S. "Removal of methylene blue from aqueous solutions by an adsorbent based on metal-organic framework and polyoxometalate", *J. Alloy. Compd.*, **648**, pp. 986-993 (2015).
29. Dod, R., Banerjee, G., and Saini, S. "Adsorption of methylene blue using green pea peels (Pisum sativum): A cost-effective option for dye-based wastewater treatment", *Biotechnol. Bioproc. E.*, **17**, pp. 862-874 (2012).
30. Chowdhury, S., Balasubramanian, R., and Das, P. "Novel carbon-based nanoadsorbents for removal of synthetic textile dyes from wastewaters", *Green Chemistry for Dyes Removal from Waste Water: Research Trends and Applications*, pp. 35-82 (2015).
31. Lafi, R., ben Fradj, A., Hafiane, A., and Hameed, B.H. "Coffee waste as potential adsorbent for the removal of basic dyes from aqueous solution", *Korean J. Chem. Eng.*, **31**(12), pp. 2198-2206 (2014).
32. Chang, Y., Lai, J.Y., and Lee, D.J. "Thermodynamic parameters for adsorption equilibrium of heavy metals and dyes from wastewaters: Research updated", *Bioresource Technol.*, **222**, pp. 513-516 (2016).
33. Du, J.J., Yuan, Y.P., Sun, J.X., Peng, F.M., Jiang, X., Qiu, L.G., Xie, A.J., Shen, Y.H., and Zhu, J.F. "New photocatalysts based on MIL-53 metal-organic

frameworks for the decolorization of methylene blue dye", *J. Hazard. Mater.*, **190**(1-3), pp. 945-951 (2011).

34. Hasan, Z. and Jhung, S.H. "Removal of hazardous organics from water using metal-organic frameworks (MOFs): Plausible mechanisms for selective adsorptions", *J. Hazard. Mater.*, **283**, pp. 329-339 (2015).
35. Gürses, A., Doğar, Ç., Yalçin, M., Açikyildiz, M., Bayrak, R., and Karaca, S. "The adsorption kinetics of the cationic dye, methylene blue, onto clay", *J. Hazard. Mater.*, **131**(1), pp. 217-228 (2006).
36. Canli, M., Abali, Y., and Bayca, S.U. "Removal of methylene blue by natural and ca and k-exchanged zeolite treated with hydrogen peroxide", *Physicochem. Probl. Mi.*, **49**, pp. 481-496 (2013).
37. Doğan, M., Abak, H., and Alkan, M. "Biosorption of methylene blue from aqueous solutions by hazelnut shells: Equilibrium, parameters and isotherms", *Water, Air, Soil Poll.*, **192**(1-4), pp. 141-153 (2008).
38. Sarici-Ozdemir, C. "Adsorption and desorption kinetics behaviour methylene blue onto activated carbon and silver activated carbon", *New Biotechnol.*, **29**, S177 (2012).
39. Liu, T., Li, Y., Du, Q., Sun, J., Jiao, Y., Yang, G., Wang, Z., Xia, Y., Zhang, W., Wang, K., Zhu, H., and Wu, D. "Adsorption of methylene blue from aqueous solution by graphene", *Colloid. Surfaces B: Biointerfaces*, **90**, pp. 197-203 (2012).
40. Li, Y., Du, Q., Liu, T., Peng, X., Wang, J., Sun, J., Wang, Y., Wu, S., Wang, Z., Xia, Y., and Xia, L. "Comparative study of methylene blue dye adsorption onto activated carbon, graphene oxide, and carbon nanotubes", *Chem. Eng. Res. Des.*, **91**(2), pp. 361-368 (2013).
41. Shao, Y., Zhou, L., Bao, C., Ma, J., Liu, M., and Wang, F. "Magnetic responsive metal-organic frameworks nanosphere with core-shell structure for highly efficient removal of methylene blue", *Chem. Eng. J.*, **283**, pp. 1127-1136 (2016).
42. Zhang, C.-F., Qiu, L.-G., Ke, F., Zhu, Y.-J., Yuan, Y.-P., Xu, G.-S., and Jiang, X. "A novel magnetic recyclable photocatalyst based on a core-shell metal-organic framework Fe_3O_4@MIL-100(Fe) for the decolorization of methylene blue dye", *J. Mater. Chem. A*, **1**(45), p. 14329 (2013).
43. Foo, K.Y. and Hameed, B.H. "Insights into the modeling of adsorption isotherm systems", *Chem. Eng. J.*, **156**, pp. 2-10 (2010).
44. Njoku, V.O., Foo, K.Y., Asif, M., and Hameed, B.H. "Preparation of activated carbons from rambutan (nephelium lappaceum) peel by microwave-induced KOH activation for acid yellow 17 dye adsorption", *Chem. Eng. J.*, **250**, pp. 198-204 (2014).
45. Rondon, W., Freire, D., De Benzo, Z., Sifontes, A.B., Gonzalez, Y., Valero, M., and Brito, J.L. "Application of 3A zeolite prepared from venezuelan kaolin for removal of Pb (II) from wastewater and its determination by flame atomic absorption spectrometry", *Am. J. Anal. Chem.*, **4**, pp. 584-593 (2013).
46. Kumar, M. and Tamilarasan, R. "Modeling of experimental data for the adsorption of methyl orange from aqueous solution using a low cost activated carbon prepared from Prosopis", *Pol. J. Chem. Technol.*, **15**(2), pp. 29-30 (2013).

Appendix A

Freundlich, Temkin and D-R parameters of MB adsorption isotherms

The Freundlich isotherm is an empirical equation which assumes that the adsorption process occurs on a heterogeneous surface via a multilayer adsorption mechanism, and adsorption capacity is related to the concentration of dye at equilibrium. The linear form of the Freundlich model can be expressed by Eq. (A.1) [43]:

$$\ln q_e = \frac{1}{n} \ln C_e + \ln K_F, \tag{A.1}$$

where K_F (L/g) and n are the adsorption constants that indicate the adsorption capacity; the value of $\frac{1}{n}$ ranging from 0.1 to 1.0 demonstrates a favorable adsorption condition. A linearity between $\ln q_e$ and $\ln C_e$ is obtained, which is shown in Figure A.1 from the slope and intercept of the regression; the values of Freundlich parameters (K_F and n) are calculated and listed in Table 1.

The Temkin isotherm is based on an assumption that there is an indirect adsorbate-adsorbate interaction for adsorption. The heat of adsorption slakes linearly with coverage due to this interaction. The linear form of the Temkin isotherm model can be expressed by Eq. (A.2) [44]:

$$q_e = B_T \ln K_t + B_T \ln C_e, \tag{A.2}$$

where $B_T = \frac{RT}{b_T}$, and b_T (J/mol) is the Temkin constant related to the heat of adsorption; R is the universal gas constant (8.314 J/mol.K); T is the

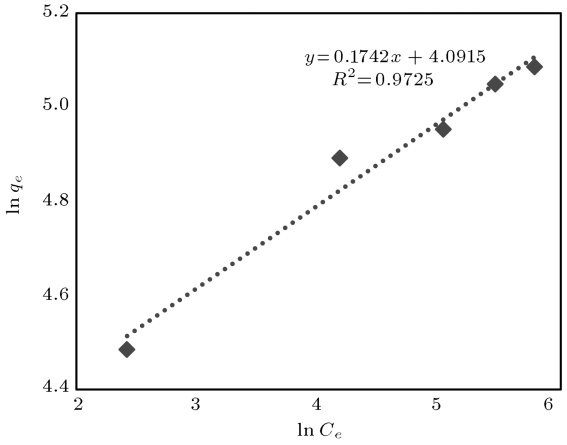

Figure A.1. Linear plot of Freundlich isotherm of MB adsorption onto Fe-MOF-5.

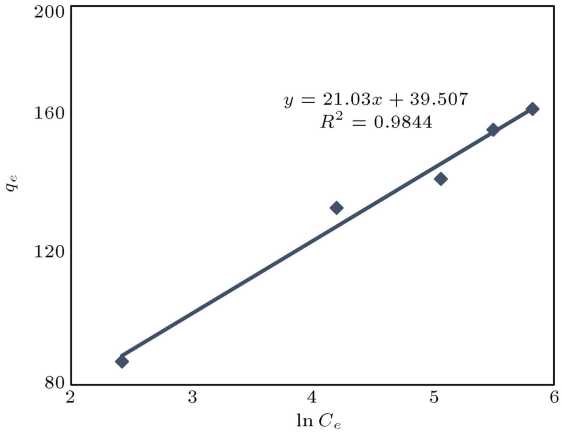

Figure A.2. Linear plot of Temkin isotherm of MB adsorption onto Fe-MOF-5.

temperature (K); K_t is the maximum binding energy constant, and q_e (mg/g) and C_e (mg/L) are the value of adsorbate adsorbed onto the adsorbent and the adsorbate concentration at equilibrium, respectively. A linear regression plot of q_e versus ln C_e is shown in Figure A.2, and the calculated values of B_T, b_T, and K_t were included in Table 1.

This isotherm does not consider constant adsorption possibility or homogeneous surface for the adsorbent [45]. Thus, the D-R linear form (Eq. (A.3)) can be applied on both homogeneous and heterogeneous surfaces:

$$\ln q_e = \ln q_m - \beta\varepsilon^2, \tag{A.3}$$

where β (mol^2.K/J^2) is a constant related to the mean free energy of adsorption, q_m (mg/g) is the theoretical saturation capacity based on D-R isotherm, and ε can be calculated from the Eq. (A.4):

$$\varepsilon = RT \ln\left(1 + \frac{1}{C_e}\right), \tag{A.4}$$

where ε is the D-R isotherm constant. Figure A.3 represents the plot of ln q_e against ε^2 for adsorption of MB onto Fe-MOF-5, which allows for determining q_m and β from the intercept and the slope, respectively. The value of mean adsorption energy, E_a (KJ/mol), can be calculated from D-R parameter β as in Eq. (A.5) [45]:

$$E_a = \frac{1}{\sqrt{2\beta}}. \tag{A.5}$$

Appendix B

Pseudo-first-order and Elovich kinetic models

The linearized-integral form of the pseudo-first-order model is as in Eq. (B.1) [46]:

$$\log(q_e - q_t) = \log q_e - \frac{k_L}{2.303}t, \tag{B.1}$$

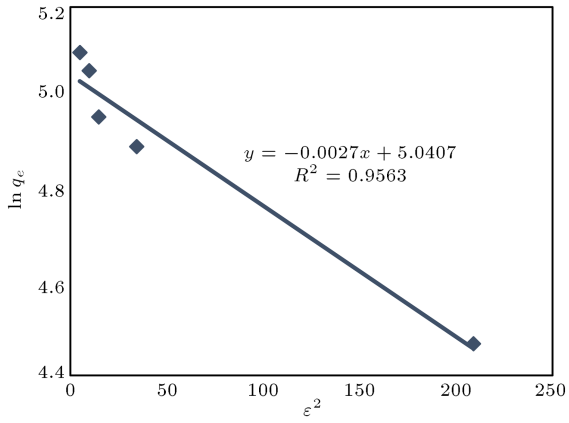

Figure A.3. Linear plot of D-R isotherm of MB adsorption onto Fe-MOF-5.

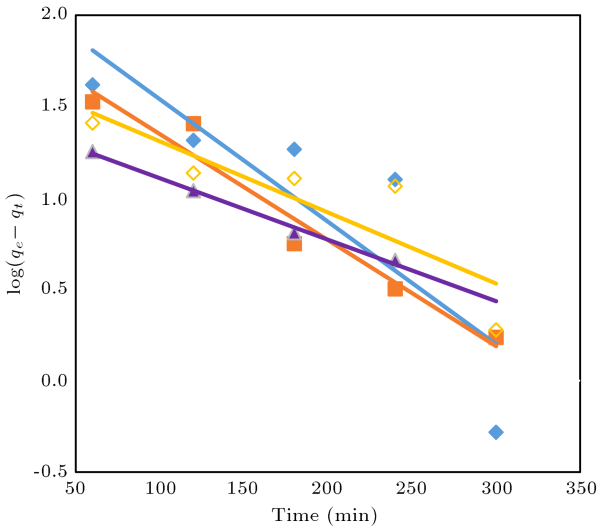

Figure B.1. Linear plot of pseudo-first-order kinetic model of MB adsorption onto Fe-MOF-5 (C_0 = ♦100 mg/L, ■ 200 mg/L, ▲ 300 mg/L, ◊ 400 mg/L).

where q_e and q_t are the adsorption capacity of Fe-MOF-5 for MB at equilibrium and any instant of time (min), respectively. K_L is the rate constant of pseudo-first-order adsorption (min^{-1}). K_L and q_e are calculated from the slope and intercept of the plots of $\log(q_e - q_t)$ versus t, respectively (Figure B.1).

The linear form of the Elovich model is presented by Eq. (B.2) [46]:

$$q_t = \frac{1}{\beta}\ln(\alpha\beta) + \frac{1}{\beta}\ln(t). \tag{B.2}$$

The constants α and β were obtained from the slope and intercept of the linear plot of q_t versus $\ln(t)$, as shown in Figure B.2; the values are presented in Table 2. The low correlation coefficient, R^2, also shows that the adsorption of MB onto Fe-MOF-5 poorly fits the Elovich kinetic model.

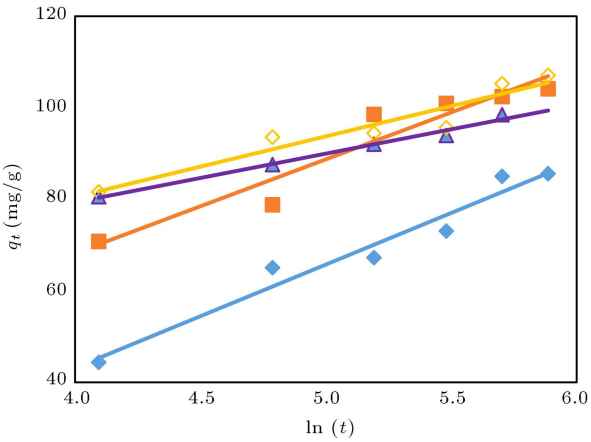

Figure B.2. Linear plot of Elovich kinetic model of MB adsorption onto Fe-MOF-5 (C_0 = ♦100 mg/L, ■ 200 mg/L, ▲ 300 mg/L, ◊ 400 mg/L).

Biographies

Abdollah Fallah Shojaei was born in Qum, Iran in 1968. He obtained a BS degree in Applied Chemistry from University of Tehran and received his MS and PhD degrees in Inorganic Chemistry from Shahid Beheshti University and University of Isfahan in 1991 and 2004, respectively. He is currently a Full Professor in Inorganic Chemistry at University of Guilan, Iran. His current research interests include bioinorganic chemistry, nano-catalysis, photodegradation and applications of metal-organic frameworks as an adsorbent.

Khalil Tabatabaeian was born in Mashhad, Iran in 1953. He received his BS degree in Pure Chemistry from Ferdowsi University of Mashhad, Iran in 1976 and obtained his PhD degree in Inorganic Chemistry from Sheffield University, England in 1980. He has been a Full Professor at University of Guilan since 1982. His current research interests include heterogenization of homogeneous catalysts, through covalent attachment to inorganic matrices such as zeolites and metal-organic frameworks combining the advantages of homogenous and heterogeneous catalyses.

Mahshid Zebardast was born in Tehran, Iran in 1986. She received her BS degree in Applied Chemistry from Payam-e-Noor University of Tehran, Iran in 2009 and also an MS degree in Inorganic Chemistry from Khajeh Nasir University of Technology, Iran in 2011. Currently, she is working on her PhD program under supervision of Dr. Fallah Shojaei and Dr. Tabatabaeian at University of Guilan. Her Current research interests include adsorptive removal of organic and inorganic pollutants from water with modified-metal-organic frameworks.